Article

Synthesis and Preclinical Evaluation of the First Carbon-11 Labeled PET Tracers Targeting Substance P

Aleksandra Pekosak, Janez Ž. Bulc, Špela Korat, Robert C. Schuit, Esther Kooijman, Ricardo Vos, Marissa Rongen, Mariska Verlaan, Kevin Takkenkamp, Wissam Beaino, Alex J. Poot, and Albert D. Windhorst

Mol. Pharmaceutics, **Just Accepted Manuscript** • DOI: 10.1021/acs.molpharmaceut.8b00518 • Publication Date (Web): 18 Oct 2018

Synthesis and Preclinical Evaluation of the First Carbon-11 Labeled PET Tracers Targeting Substance P_{1-7}

Aleksandra Pekošak, Janez Ž. Bulc[§], Špela Korat[§], Robert C. Schuit, Esther Kooijman, Ricardo Vos, Marissa Rongen, Mariska Verlaan, Kevin Takkenkamp, Wissam Beaino, Alex J. Poot, Albert D. Windhorst

Department of Radiology and Nuclear Medicine, VU University Medical Center, Amsterdam, the Netherlands

Abstract:

Two potent SP_{1-7} peptidomimetics have been successfully radiolabeled via $[^{11}C]CO_2$-fixation in excellent yields, purity and molar activity. L-$[^{11}C]SP_{1-7}$-peptidomimetic exhibited promising *ex vivo* biodistribution profile. Metabolite analysis showed that L-$[^{11}C]SP_{1-7}$-peptidomimetic is stable in brain and spinal cord, whereas rapid metabolic degradation occurs in rat plasma. Metabolic stability can be significantly improved by substituting L-Phe for D-Phe, preserving 70% more of intact tracer and resulting in better brain and spinal cord tracer retention. PET scanning confirmed moderate brain (1.5 SUV; peak at 3 min) and spinal cord (1.0 SUV; peak at 10 min) uptake for L- and D-$[^{11}C]SP_{1-7}$-peptidomimetic. A slight decrease in SUV value was observed after pretreatment with natural peptide SP_{1-7} in spinal cord for L-$[^{11}C]SP_{1-7}$-peptidomimetic. On the contrary, blocking using cold analogues of L- and D-$[^{11}C]$tracers did not reduce the tracers' brain and spinal cord exposure. In summary, PET scanning of L- and D-$[^{11}C]SP_{1-7}$-peptidomimetics confirms rapid blood-brain-barrier and blood-spinal-cord-barrier penetration. Therefore, further validation of these two tracers targeting SP_{1-7} is needed in order to define a new PET imaging target and select its most appropriate radiopharmaceutical.

Table of Contents

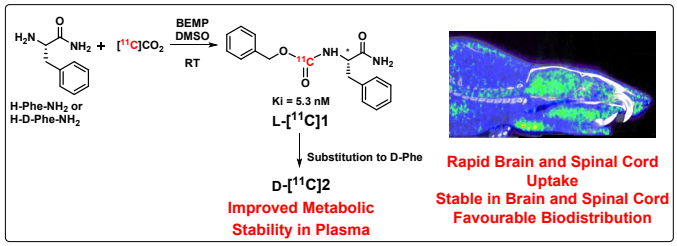

Keywords: Substance P_{1-7}, CO_2 fixation, Carbon-11, Metabolism, Biodistribution, PET Imaging

Introduction

Substance P (SP) (H-Arg-Pro-Lys-Pro-Gln-Gln-Phe-Phe-Gly-Leu-Met-NH_2) is a neurotransmitter and neuromodulator involved in a variety of neurological functions. Its role in pain transmission has attracted particular interest, since SP binds preferably to the neurokinin 1 receptor (NK-1R), however the SP *N*-terminal major bioactive fragment SP_{1-7} (H-Arg-Pro-Lys-Pro-Gln-Gln-Phe-OH) acts through binding to a specific site apart from any known neurokinin or opioid receptor. The absence of binding of SP_{1-7} to the NK-1R is attributed to the lack of the amidated amino acid sequence Gly^9-Leu^{10}-Met^{11}-NH_2 on the *C*-terminus.[1–7]

SP_{1-7} has been shown to be present in various central nervous system (CNS) areas, such as hypothalamus, nucleus accumbens, ventral tragemental area, and in the dorsal and ventral part of spinal cord, confirming that the heptapeptide is related to pain and reward processing when produced in the CNS by endopeptidases. [8–10] Even though the binding sites in mouse and rat are known, the receptor for SP_{1-7} has not yet been cloned or characterized, making its mechanism of action remaining unclear.[8,11] Recently, *in vitro* and *in vivo* studies showed improved binding affinity of amidated *C*-terminus SP_{1-7}-NH_2 compared to the endogenous fragment SP_{1-7}, as well as increased potency effect to mediate a reduced expression of opioid withdrawal through the SP_{1-7} binding site.[12,13] In addition, the SP_{1-7} analog D-SP_{1-7} (D-Pro^2-D-Phe^7-SP_{1-7}) was able to block SP_{1-7} induced antinociception and showed binding affinity to SP_{1-7} binding site equipotent to natural SP_{1-7}.[1,14,15] Interestingly, the SP_{1-7}-NH_2 showed higher anti-allodynic activity after intraperitoneal administration compared to SP_{1-7} despite the poor *in vivo* stability of both peptides.[7]

Aiming to develop a peptidomimetic with a long duration of action and be able to cross the blood-brain barrier (BBB), Fransson *et al.* performed extensive structure-activity relationship (SAR) studies resulting in a lead dipeptide H-Phe-Phe-NH_2 (K_i of 1.5 nM; rat spinal cord membrane) as small molecule to target the SP_{1-7} binding site.[5,12] Further fine-tuning, by replacing the *N*-terminal Phe with a benzylcarbamate group, resulted in a peptidomimetic (*S*)-benzyl (1-amino-1-oxo-3-phenylpropan-2-yl)carbamate **L-1** with a K_i of 5.2 nM, determined by using rat spinal cord membranes preparation (Figure 1).[1,11,16] Its reasonable binding affinity, excellent membrane permeability, low efflux, moderate *in vitro* clearance and ability to enter the CNS according to the *in vivo* infusion study, make SP_{1-7} an interesting target for PET tracer development.

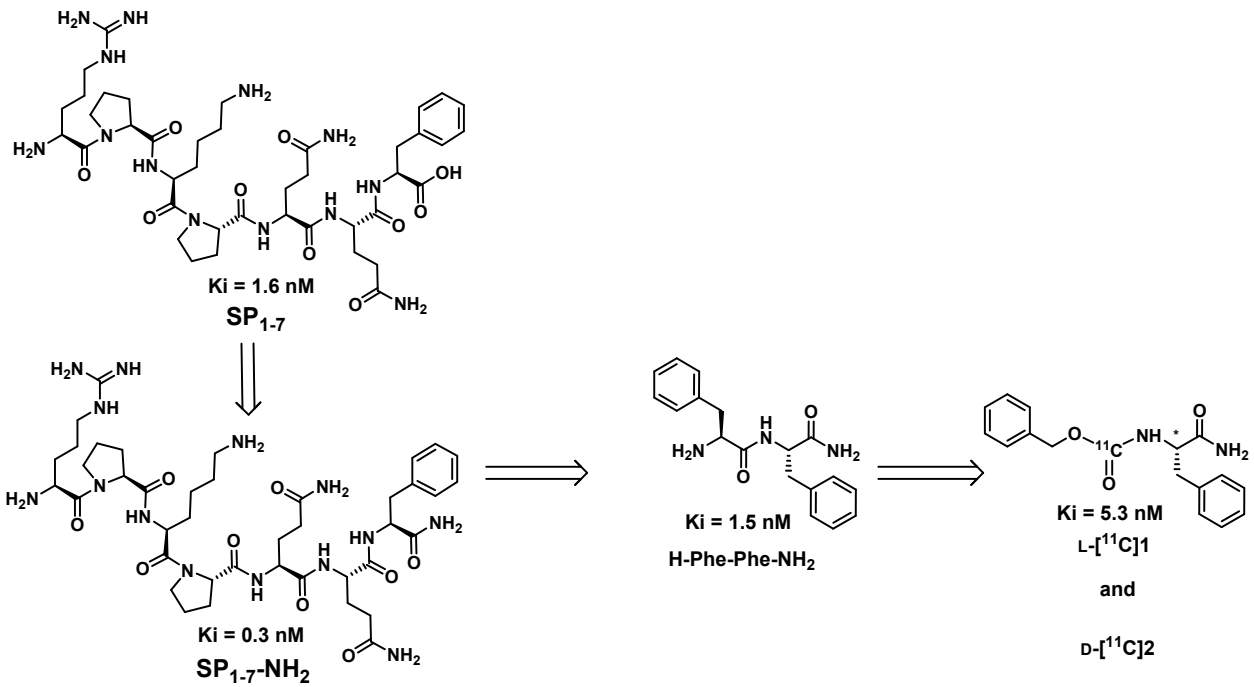

Figure 1: Structure of SP_{1-7} and SP_{1-7}-NH_2 as leads for the development of small molecules, H-Phe-Phe-NH_2 and the peptidomimetics **L-1** and **D-2**. Red ^{11}C indicates radiolabeling position using the $[^{11}C]CO_2$-fixation method.

Neuropathic pain is clinically characterized by spontaneous and evoked type of pain significantly impairing the quality of patients' life whereas its effect in treating represents a major unsolved problem.[17] Developing PET-tracers able to image and evaluate neuropathic pain would provide a valuable tool for better estimation of the incidence and prevalence of neuropathic pain, and treatment development.[18] SP_{1-7} is a relatively large molecule and current radiolabeling techniques require a strong modification of the native peptide structure hampering the BBB penetration. Nonetheless, the dipeptide peptidomimetics are more attractive alternative and could be viable neuro PET tracers able to cross the BBB. PET imaging is a powerful technique that provides direct quantitative information on the levels of brain and spinal cord exposure, target engagement and pharmacological activity.[19,20] In our study, we used dipeptide peptidomimetics (Figure 1) for radiolabeling with carbon-11 in order to investigate the SP_{1-7} binding site and provide insights in the potential neuropathic pain PET imaging.

The merits of carbon-11 ($t_{1/2}$=20.4 min, 99% β+, 0.96 MeV) as a choice radionuclide for PET tracer synthesis have been well recognized. The ubiquity of carbon atoms in all pharmacologically active compounds makes it an attractive isotope for radiolabeling, preserving the favorable physicochemical properties.[21–28] With the recent developments in carbon-11 chemistry, routinely employed complex processes and appropriate special equipment, radiochemists are able to label various compounds. Direct fixation of $[^{11}C]CO_2$, published by Hooker *et al.*[29] and Wilson *et al.*[30], addressing the carbon-11 labeled carbamate functional group, enables us to label the SP_{1-7} peptidomimetic (*S*)-benzyl (1-amino-1-oxo-3-phenylpropan-2-yl)carbamate **L-1** or (*R*)-benzyl (1-amino-1-oxo-3-phenylpropan-2-yl)carbamate **D-2** (Figure 1) to serve as a research tool to investigate the SP_{1-7} binding site. To achieve this goal, we firstly investigated their physiochemical

properties using novel tool CNS PET multi parameter optimization (MPO) algorithm[31,32], as well as commercial platform for *in silico* prediction of physicochemical, absorption, distribution, metabolism, and excretion (ADME), and toxicity properties, to provide valuable information if compounds of interest meet a distinctive set of criteria for CNS PET ligand. As prediction models provided enviable starting point for PET ligand discovery effort, we investigated the feasibility of carbon-11 radiolabeling of compounds **1** and **2** without further modifications. Finally, we evaluated their biodistribution, *in vivo* metabolic stability and assessed their *in vivo* behavior in brain and spinal cord using PET imaging.

Experimental Section

Materials and Methods

Chemicals were obtained commercially from Sigma-Aldrich (Zwijndrecht, the Netherlands) and Bachem (Bubendorf, Switzerland), and used without further purification, unless stated otherwise. Solvents were purchased from Biosolve (Valkenswaard, the Netherlands) and Acros (Landsmeer, the Netherlands), and used as received, unless stated otherwise. All deuterated solvents were purchased from Sigma-Aldrich (Zwijndrecht, the Netherlands). Reactions were performed at ambient temperature unless stated otherwise and monitored by thin layer chromatography on pre-coated silica 60 F_{254} aluminum plates (Merck, Darmstadt, Germany). Spots were visualized by UV light (254 nm) and ninhydrine or bromocresol green staining. Solvents were evaporated under reduced pressure using a rotary evaporator (Rotavapor® R II, Flawil, Switzerland). Flash column chromatography was performed on Büchi (Flawil, Switzerland) Sepacore system (comprising a C-620 control unit, a C-660 fraction collector, two C-601 gradient pumps and a C-640 UV detector)

equipped with Büchi Sepacore pre-packed flash columns. Yields refer to purified and spectroscopically pure compounds.

NMR spectroscopy was performed on a Bruker Avance 250, 400 or 500 MHz spectrometer (Billerica, MA, USA, exact magnetic field is reported in the chemical syntheses section) with chemical shifts (δ) reported in parts per million (ppm) relative to the solvent ($CDCl_3$, ^1H 7.26 ppm, ^{13}C 77.16 ppm; D_2O, ^1H 4.79 ppm; $(CD_3)_2SO$, ^{13}C 39.52 ppm). Splitting patterns are indicated as s: singlet, d: doublet, t: triplet, q: quartet, m: multiplet and br: broad peak, and *J*, coupling constant in Hz. Electrospray ionization-high resolution mass spectrometry (ESI-HRMS) was carried out using Bruker microTOF-Q instrument in a positive ion mode (capillary potential of 4500 V) and interpreted with Bruker Compass Data Analysis 4.0 software.

Analytical HPLC was performed on a Shimadzu SPD-20A system (Shimadzu Corporation, Japan) and Jasco PU-2089 Plus station (Easton, MD, USA) with a Alltima C18 5 μm (250 × 4.6 mm) column (Grace, Breda, the Netherlands) (A) with Jasco UV-2075 Plus UV detector (254 nm) and NaI radioactivity detector (Raytest, Straubenhardt, Germany) at ambient temperature with a flow rate 1 $mL \cdot min^{-1}$. Acetonitrile (C), acetonitrile+0.1% TFA (D), water (E), water+0.1% TFA (F) and buffer 1 (4 mM sodium formate and 4% dimethylformamide) (G) were used as mobile phases. Chromatograms were acquired with LabSolutions 5.85 software (Shimadzu Corporation, Japan) and Raytest GINA Star software (version 5.8; Straubenhardt, Germany).

*Method A: solvents D/F (*v*/*v*), linear gradient, 0 - 1 min: 35% D; 1 - 19 min: 35-65% D; 19 - 20 min: 65 - 35% D; 20 - 21 min: 65% D.

Semi-preparative isocratic HPLC was performed on Jasco UV-2087 Plus station with a Alltima C18 5 μm (250 × 10 mm) column (Grace, Breda, the Netherlands) (J) using C/G (40/60, *v*/*v*) as a

eluent, flow rate 5 mL·min^{-1} (Method B), a Jasco UV-2075 Plus UV detector (254 nm), a homemade radioactivity detector and Jasco ChromNAV CFR software (version 1.14.01).

HPLC conditions for metabolite analysis and LC-MS/MS analysis are for convenience reported under appropriate section.

Prediction Models:

- **ACD Labs - Percepta**

Full array of physiochemical, ADME and toxicity properties, next to BBB transport parameters were predicted using the commercial package of ACD/Percepta (version: 14.2.0 (Build 2972)).

- **CNS PET Multi Parameter Optimization (MPO)**

CNS PET MPO value was calculated using a set of six physiochemical parameters:

- molecular weight (MW),
- lipophilicity, calculated partition coefficient (ClogP),
- calculated distribution coefficient at pH=7.4 (ClogD),
- topological polar surface area (tPSA),
- ionization constant of the most basic center (pKa) and
- number of hydrogen bond donors (HBD).

following the publication of Zhang *et al.*[31] and standard commercial packages described in the paper of Wager *et al.*[33]:

List of standard commercial packages: Biobyte (Bio-Loom; version 5) for ClogP, ACD/Percepta for ClogD at pH=7.4, tPSA, pKa, ChemDraw (professional; version: 16.0.1.4 (77)) for Mw and HBD.

Calculation of the Radiochemical Yield by Analytical HPLC

Radiochemical yield, determined by analytical HPLC of the crude reaction mixture, defined as radiochemical conversion (RCC), was determined by HPLC as the percentage of converted [^{11}C]CO_2 to desired product [^{11}C]**1** or [^{11}C]**2** in the crude reaction mixture using an analytical HPLC method described in the radiochemistry section under each procedure and is based on the area under the curve (AUC) of the radioactivity profile of HPLC analysis.

Calculation of the Radiochemical Yield

Radiochemical yield (RCY) was calculated as the quotient of measured activity of the isolated product at the end of the synthesis (EOS) and the measured activity at the end of the cyclotron bombardment (EOB) and expressed as a percentage. Radiochemical yield has been corrected for decay from the EOB. No corrections have been made for material losses (potentially volatile radioactive species or residual activity in the vial, tubes and syringes).

Calculation of the Molar Activity

Molar activity (A_M) of the final tracer, expressed as $GBq \cdot \mu mol^{-1}$, was determined by measurement of the UV absorbance (AUC) of a known amount of radioactivity under identical analytical HPLC conditions used to generate a mass calibration curve for the corresponding non-radioactive standard.

The Mass Calibration Curve

The mass calibration curve was performed using samples of the reference compound **1** due to strong UV absorption and is based on the AUC of HPLC analysis.

Chemical Syntheses:

***(S)*-benzyl (1-amino-1-oxo-3-phenylpropan-2-yl)carbamate (1)**

Starting compound *(S)*-2-(((benzyloxy)carbonyl)amino)-3-phenylpropanoic acid (80.0 mg, 267 µmol, 1 eq) and di-*tert*-butyl dicarbonate (125 mg, 573 µmol, 2 eq) were dissolved in 3 mL of 1,4-dioxane and placed on a magnetic mixer. Pyridine (18.0 µL, 267 µmol, 1 eq) and ammonium hydrogen carbonate (58.0 mg, 746 µmol, 2.8 eq) were added to the solution. The reaction mixture was flushed with nitrogen and left stirring overnight (17 h). Solvents were evaporated *in vacuo*. The remaining material in the vessel was dissolved in 7 mL of ethyl acetate (EtOAc), washed three times with 5 mL of 5 mM H_2SO_4 and three times with 5 mL of brine. The organic phases were combined, dried over $MgSO_4$, filtered and evaporated *in vacuo*. Compound **1** was obtained in 80% yield as a white crystalline powder after precipitation in ice-cold *n*-hexane. ^{1}H NMR (250.13 MHz, DMSO-d_6): δ (ppm) = 7.50 (br s, 1H, -N<u>H</u>-), 7.31 – 7.19 (m, 10H, 10x Ar-<u>H</u>), 7.07 (s, 2H, -N<u>H</u>$_2$), 4.91 (s, 2H, -C<u>H</u>$_2$-O), 4.19 – 4.10 (m, 1H, -C<u>H</u>-CH$_2$-), 3.00 (dd, J_1=22 Hz, J_2=8 Hz, 1H, C<u>H</u>$_2$-CH-), 2.75 – 2.66 (m, 1H, C<u>H</u>$_2$-CH-). ^{13}C NMR (125.81 MHz, DMSO-d_6): δ (ppm) = 174.05 (-<u>C</u>ONH$_2$), 160.09 (-<u>C</u>OONH-), 138.61 (Ar), 129.61 (Ar), 128.76 (Ar), 128.53 (Ar), 127.85 (Ar), 126.74 (Ar), 74.94 (-<u>C</u>H$_2$O-), 65.64 (-<u>C</u>H-), 37.91 (-CH$_2$CH-). HRMS: Calculated for $C_{17}H_{18}N_2O_3$ 298.1317, measured 299.1225 ($M+H^+$) and 321.1225 ($M+Na^+$). HPLC purity: >99% (determined by HPLC: column A, method A, R_t = 11.8 min).

Synthesis of *(R)*-benzyl (1-amino-1-oxo-3-phenylpropan-2-yl)carbamate (2)

Starting compound *(R)*-2-(((benzyloxy)carbonyl)amino)-3-phenylpropanoic acid (100 mg, 334 µmol, 1 eq) and di-*tert*-butyl dicarbonate (183 mg, 668 µmol, 2 eq) were dissolved in 3 mL of 1,4-dioxane and placed on a magnetic mixer. Pyridine (27.0 µL, 334 µmol, 1 eq) and ammonium

hydrogen carbonate (75.0 mg, 868 µmol, 2.6 eq) were added to the solution. Nitrogen athmosphere was introduced before the solution was left stirring overnight (18 hrs). Solvents were evaporated *in vacuo*. The remaining material in the vessel was dissolved in 7 mL of EtOAc, washed three times with 5 mL of 5 mM H_2SO_4 and three times with 5 mL of brine. The organic phases were combined, dried over $MgSO_4$, filtered and evaporated *in vacuo*. Compound **2** was obtained in 55% yield as a white crystalline powder after precipitation in ice-cold *n*-hexane. ^{1}H NMR (400.13 MHz, DMSO-d_6): δ (ppm) = 7.47 (br s, 1H, -NH-), 7.41 – 7.21 (m, 10H, 10x Ar-H), 7.07 (s, 2H, -NH_2), 4.94 (s, 2H, -CH_2-O), 4.19 – 4.16 (m, 1H, -CH-CH_2-), 3.00 (dd, J_1=16 Hz, J_2=4 Hz, 1H, CH_2-CH-), 2.74 (t, J=12 Hz, 1H, CH_2-CH-). ^{13}C NMR (125.81MHz, DMSO-d_6): δ (ppm) = 173.88 (-$CONH_2$), 153.30 (-COONH-), 138.77 (Ar), 137.52 (Ar), 128.93 (Ar), 128.73 (Ar), 128.49 (Ar), 127.88 (Ar), 126.66 (Ar), 65.58 (-CH_2O-), 65.54 (-CH-), 37.96 (-CH_2CH-). HRMS: Calculated for $C_{17}H_{18}N_2O_3$ 298.1317, measured 299.1378 $(M+H)^+$ and 321.1199 $(M+Na)^+$. HPLC purity: >95% (determined by HPLC: column A, method A, R_t = 11.8 min).

Radiosynthesis:

Radionuclide production procedure for carbon-11

An IBA Cyclone 18/9 (IBA, Louvain-la Neuve, Belgium) cyclotron was used for [^{11}C]CO_2 production by the ^{14}N(p,α)^{11}C nuclear reaction performed in a 0.5% O_2/N_2 gas mixture. After trapping of [^{11}C]CO_2 from the target in a stainless trap dispersed in liquid N_2, [^{11}C]CO_2 was transferred to the desired reaction vessel using a 10 mL·min^{-1}helium flow.

Procedure of the manual synthesis of *(S)*-[^{11}C]benzyl (1-amino-1-oxo-3-phenylpropan-2-yl)carbamate

H-L-Phe-NH_2 was placed in a pre-dried reaction vessel in a research hot-cell and dissolved in DMSO containing BEMP. [^{11}C]CO_2 (4 - 6 GBq) was transferred through a sicapent (phosphorus pentoxide) column to the mixture using helium flow of 10 mL·min^{-1} from a CO_2 trap. When the activity in the vessel reached its maximum, DMSO containing benzyl chloride was manually added to the reaction vessel with a syringe, heated to 75 °C and left to stir with helium flow (10 mL·min^{-1}) for 2 - 10 min. Approximately 50 µL of the reaction mixture was then quenched with 300 µL of solution of acetonitrile and water (1/1; *v/v*) and analyzed on HPLC (Column A; Method A) to determine the radiochemical yield expressed as radiochemical conversion of the reaction.

Procedure for the automated synthesis of *(S)*-[^{11}C]benzyl (1-amino-1-oxo-3-phenylpropan-2-yl)carbamate ([^{11}C]1) and of *(R)*-[^{11}C]benzyl (1-amino-1-oxo-3-phenylpropan-2-yl)carbamate ([^{11}C]2)

L-Phe-NH_2 or D-Phe-NH_2 (1.0 mg, 3.3 µmol) was placed in a pre-dried reaction vessel dissolved in DMSO (0.15 mL) containing BEMP (8.3 µL) and fixed in the home-build synthesis module located in the hot-cell.[34] [^{11}C]CO_2 (45 GBq) was transferred through a sicapent column to the mixture using helium flow (10 mL·min^{-1}). When the activity in the vessel reached its maximum, benzyl chloride (4.0 µL) in DMSO (0.15 mL) was automatically added to the reaction vessel, which was then heated to 75 °C and left to stir with helium (10 mL·min^{-1}) for 5 min. The mixture was then cooled to 25 °C, quenched with a solution of acetonitrile and water (1/1; *v/v*; 1.5 mL) and injected on a preparative HPLC column (Column J, Method B). The product, eluting between 12 and 14 min, was collected (Supporting information: Figure 2), diluted in 7 mL of water and loaded on a pre-conditioned Sep-Pak C_{18} column. The Sep-Pak C_{18} column was washed with 5 mL of

water, before the product was eluted with 1 mL of ethanol (EtOH). Saline solution (9 mL) was added to the product, forming the final injectable radioactive tracer.

[^{11}C]**1** was obtained in a decay-corrected radiochemical yield of 27.9 ± 10.9% (n=10) with an isolated non-decay-corrected yield of 5.1 ± 2.2 GBq (n=10) of the product with a radiochemical purity >99%, an average A_M of 93.2 ± 46.9 GBq·μmol^{-1} (n=9) within 24 - 26 min (n>10). The identity of the product was confirmed with analytical HPLC (Column A; Method A) by co-injection of the product and non-labeled **1** (Supporting information: Figure 3).

[^{11}C]**2** was obtained in a decay-corrected radiochemical yield of 25.5 ± 9.7% (n=5) with an isolated non-corrected yield of 3.9 ± 1.9 GBq (n=5) of the product with a radiochemical purity >99%, an average A_M of 69.4 ± 11.4 GBq·μmol^{-1} (n=4) within 23 - 29 min (n=5). The identity of the product was confirmed with analytical HPLC (Column A; Method A) by co-injection of the product and non-radiolabeled **2**.

Animals

Adult healthy male Wistar rats (200 – 360 g; 7 – 10 weeks; Charles River International Inc, Sulzfeld, Germany) were housed in groups of maximal 6 in a conventional cage and kept in a ambient with a 12-hour light/dark cycle, and constant ambient temperature (19 - 21 °C) and humidity level (52 - 70%). Rats were provided with water and food pellets (Teklad Global Diet 2016, Envigo; Horst, the Netherlands) *ad libitum*. The rats were allowed to adapt to the laboratory environment for one week before the experiment. Animal experiments were performed in accordance with the European Community Council Directive (2010/63/EU) for laboratory animal care and the Dutch Law on animal experimentation. The experimental protocol was validated and approved by the local committee on animal experimentation of the VU University Medical Center.

Ex vivo Biodistribution

Healthy male Wistar rats (200 - 250 g) were injected with the radiotracer (25.8 ± 7.6 MBq; 0.74 ± 0.21 nmol; n=16) via the tail vein under isoflurane anesthesia (2 - 2.5% in 1 L·min^{-1}). Animals were sacrificed and dissected at 5, 15, 30 and 60 min (n=4 per time point) post-injection. Blood, heart, lungs, liver, kidney, duodenum, urine, tail, bone, spleen, large brain, cerebellum, brain stem, spinal cord top and spinal cord mid were collected, weighed and counted for radioactivity in a Wallac Computagama 1210 or a Wallac Universal Gamma Counter 1282. Biodistribution data are expressed as the percentage of injected dose per gram (%ID/g). Errors are standard error of the mean (SEM).

Metabolites Analysis (Plasma and Brain)

Healthy male Wistar rats (200 - 330 g) were injected with the tracer [^{11}C]**1 (**27.3 ± 7.3 MBq; 0.50 ± 0.22 nmol; n=12) or [^{11}C]**2 (**32.4 ± 3.4 MBq; 1.80 ± 0.19 nmol; n=9) via the tail vein under isoflurane anesthesia (2 – 2.5% in 1 L·min^{-1}). The rodents were sacrificed at 5, 15 and 45 min post injection for the tracer [^{11}C]**1** (n=4 per time point) and at 5, 15 and 45 min post injection for the tracer [^{11}C]**2** (n=3 per time point). Blood (2.0 - 5.0 mL) was collected via heart puncture into heparin tubes (DB Vacutainer, LH, Becton Dickinson, Franklin Lakes, NY, USA) and centrifuged at 4000 r.p.m for 5 min at 4 °C (Hettich Universal 32, Andreas Hettich GmbH & Co. KG, Tuttlingen, Germany). The brain was dissected and one hemisphere was put in a falcon tube containing 50% acetonitrile in saline (4 mL), and homogenized using a dispenser (IKA T18 B Ultra-Turrax, IKA-Werke GmbH & Co KG, Staufen, Germany) before centrifugation at 4000 r.p.m. for 5 min at 4 °C. The other hemisphere was counted for radioactivity for recovery

calculations. Plasma and brain supernatant were separated from blood cells and brain precipitate, respectively.

About 1 mL of plasma was diluted with 2 mL of 0.15 M hydrochloric acid and loaded onto a tC2 Sep-Pak cartridge, which was pre-activated by elution with 3 mL of methanol and 6 mL of water, respectively. The cartridge was washed with 3 mL of water to collect the rest of the polar radioactive metabolites. The polar radioactive metabolite fraction was defined as the two combined fractions. Next, the tC_2 Sep-Pak cartridge was eluted with 1.5 mL of methanol and 2 mL of water to collect the mixture of non-polar radioactive metabolites. About 2 mL of the brain supernatant was ultra-centrifuged (Eppendorf 5417c, Eppendorf, Hamburg, Germany) and 1 mL was injected onto an HPLC system. All non-polar metabolites and polar brain metabolites fractions were immediately analyzed using HPLC to determine the percentage of the intact [^{11}C]**1** or [^{11}C]**2**. HPLC was performed on the Dionex Ultimate 3000 System station, equipped with 1 mL loop, with Phenomenex Gemini C18, 250 × 10 mm, 5 µm, column using gradient elution of acetonitrile+0.1% TFA (D) and water+0.1% TFA (F) in water. The HPLC gradient ran for 14 min decreasing the concentration of eluent F from 90% to 20% in 11 min, 2 min with 20% of F and back to original setting (90% F) at flow 5 mL·min^{-1}. All separated fractions of the brain supernatant were counted for radioactivity in a Wizard Gamma Counter 1470 or 2480 (Wallac, PerkinElmer, Waltham, MA, USA). The percentage of the intact tracer in the non-polar plasma fractions was determined by the online radioactivity detection by HPLC analysis for [^{11}C]**1** or [^{11}C]**2** (R_t = 11.7 min). AUC, providing the percentage of the intact tracer and the metabolites, has been corrected for decay. Results are expressed as percentage of the intact tracer, polar metabolites, non-polar metabolites ± standard deviation.

Metabolites Analysis (Spinal Cord)

Healthy male Wistar rats (330 - 360 g) were injected with the tracer [^{11}C]**1** (32.8 ± 8.6 MBq; 0.63 ± 0.17 nmol; n=4) via the tail vein under isoflurane anesthesia (2 – 2.5% in 1 L·min^{-1}). The rodents were sacrificed at 15 min post injection for the tracer [^{11}C]**1** (n=4 per time point). Whole spinal cord was collected via cutting the muscles and breaking the spine, and was put in a falcon tube containing 50% acetonitrile in saline (2 mL), and homogenized with a dispenser (IKA T18 B Ultra-Turrax, IKA-Werke GmbH & Co KG, Staufen, Germany) before centrifugation at 4000 r.p.m. for 2 min at ambient temperature (Eppendorf 5417c, Eppendorf, Hamburg, Germany). Spinal cord supernatant and precipitate were separated and about 1.5 mL of was immediately analyzed using HPLC to determine the percentage of the intact [^{11}C]**1**. HPLC was consistent of the Dionex Ultimate 3000 System station, equipped with 1 mL loop, with Phenomenex Gemini C18, 250 × 10 mm, 5 μm, column using gradient elution of acetonitrile+0.1% TFA (D) and water+0.1% TFA (F). The HPLC gradient ran for 14 min decreasing the concentration of eluent F from 90% to 20% in 11 min, 2 min with 20% of F and back to original setting (90% F) at flow 5 mL·min^{-1}. The percentage of the intact tracer in the non-polar plasma fractions was determined by the online radioactivity detection by HPLC analysis for [^{11}C]**1** (R_t = 11.6 min). Area under the curve, providing the percentage of the intact tracer ot the metabolites, has been corrected for decay. Results are expressed as percentage of the intact tracer, metabolites ± standard deviation. All separated fractions (one fraction of 30 s) of the spinal cord supernatant were counted for radioactivity in a Wizard Gamma Counter 1470 or 2480 (Wallac, PerkinElmer, Waltham, MA, USA).

LC-MS/MS Method

LC–MS/MS analysis was performed on a Jasco X-LC HPLC system (Easton, PA, USA) with an AB Sciex QTRAP 5500 mass spectrometer (Concorde, Ontario, Canada). The Jasco system consisted of two pumps (X-LC 3180PU), a degasser (X-LC 3080DG), a mixer (X-LC 3080MX), a column oven (X-LC 3080CO) and an auto sampler (X-LC3159AS). Data were collected with two data boxes (LV 2080-03 and LC-Net II/ACD).

A Kinetex Biphenyl C_{18} column (2.6 μ, 100 A, 100 × 2.10 mm; Phenomenex, Torrance, CA, USA) at 25 °C was used for chromatographic separation. A gradient elution was used at a flow rate of 0.5 $mL \cdot min^{-1}$. The mobile phase consisted of a mixture of acetonitrile (C) and 0.1% formic acid in water according to the following scheme: 0 min 20% C, 90% C in 3.5 min, 90% C for 3.6 min, 20% C in 5 min at 25 ºC. MS parameters: TurboIon Spray voltage was set at 5.5 kV, source temperature at 750 °C. Based of full-scan MS and MS/MS spectra of each analyte, the most abundant fragment ions were selected and the mass spectrometer was set to monitor the transitions of the precursors to the product ions as followed: m/z 299.1 → 255.1 for the intact tracer, m/z 315.1→ 271.1 for the hydroxylated metabolite and m/z 475.1 → 299.1 for the glucoronated metabolite.

PET Imaging

Dynamic PET imaging was performed on a healthy male Wistar rats (200 – 320 g; n=10) using Nanoscan small animal PET/CT and PET/MR scanners (Mediso Ltd., Budapest, Hungary) with identical PET components. The rats were anaesthetized with 3% and 1 – 2.5% isoflurane in oxygen (1 $L \cdot min^{-1}$) for induction and maintenance, respectively. Rats were positioned on the scanner bed and respiratory rate was monitored during the entire time of scanning. A computed tomography (CT) or magnetic resonance imaging (MRI) scan was performed for 5 or 15 min, respectively,

followed by intravenous (*i.v.*) administration of [^{11}C]**1** (13.1 ± 5.8 MBq; 0.14 ± 0.06 nmol; n=4) or of [^{11}C]**2** (14.7 ± 1.5 MBq; 0.37 ± 0.24 nmol; n=3) via tail vein cannula at the start of a dynamic PET scan of 60 min. PET data were normalized, and corrected for scatter, randomization, attenuation, decay and dead time. List-mode PET data were re-binned in 18 successive frames: 4 × 5, 4 × 10, 2 × 30, 3 × 60, 2 × 300, 1 × 600, 1 × 900 and 1 × 1200 s, which were reconstructed using a fully 3-dimensional reconstruction algorithm (Tera-TomoTM) using 4 iterations and 6 subsets, resulting in an isotropic 0.4 mm voxel dimension. Static reconstruction was also performed on the total duration of the scan (60 min). Images were analyzed using the freely available AMIDE software (A Medical Image Data Examiner; version 1.0.4), whereas images in Figure 6 are made using VivoQuant (version 3.0, InVicro, Boston, MA, USA). Regions of interest (ROI) were drawn manually around whole brain (ellipsoid) and spinal cord (elliptic cylinder). Results are expressed as standardized uptake values (SUVs) and error bars indicate standard deviation using Graph Pad Prism (Version 5.02, Graph Pad Software Inc., La Jolla, CA, USA).

For blocking experiments, rats were injected with the natural heptapeptide SP_{1-7} or **1** or **2**, depending on the investigated PET tracer. The SP_{1-7} was diluted in DMSO and then further diluted with saline to the final concentration (5% DMSO). Peptide was injected intraperitoneally (*i.p.*) (185 nmol·kg^{-1}), according to previous experiments by Jonsson[1], 15 min prior to tracer [^{11}C]**1** administration (tracer administration per rat: 22.3 ± 0.5 MBq; 0.30 ± 0.01 nmol; n=2). Compound **1** was dissolved in EtOH and further diluted with saline to the final concentration (20% EtOH). **1** was injected slowly *i.v.* in the tail vein (3 μmol·kg^{-1}), according to previous experiments by Fransson[35], 3 and 20 min prior to tracer [^{11}C]**1** administration (tracer administration per rat: 34.0 ± 10.8 MBq; 0.55 ± 0.14 nmol; n=3 for 3 min and 16.4 ± 4.3 MBq; 0.22 ± 0.04 nmol; n=2 for 20 min). Same dose and formulation conditions applied for compound **2**, with the exception that it

was injected only 3 min prior to tracer [^{11}C]**2** administration (tracer administration per rat: 16.8 ± 10.1 MBq; 0.25 ± 0.15 nmol; n=2).

Results

Prediction Models

The characteristics of the SP_{1-7} peptidomimetics for brain penetration were anticipated prior to synthesis and radiolabeling. ACD/Labs Percepta's Drug profiler and BBB module report confirmed optimal physiochemical and ADME profile, as well as brain penetration sufficient for CNS activity (Supporting Information). CNS PET MPO algorithm was calculated following the publication of Zhang *et al.*[31] and displayed value of 3.6, which is in the desirable range for BBB penetration (Supporting Information).

Chemistry

Reference compounds ((*S*)-benzyl (1-amino-1-oxo-3-phenylpropan-2-yl)carbamate **1** and ((*R*)-benzyl (1-amino-1-oxo-3-phenylpropan-2-yl)carbamate **2**) were synthesized according to patented procedure[36] in a one-step amidation reaction (Supporting Information; Scheme 1) from a commercially available 2-(((benzyloxy)carbonyl)amino)-3-phenylpropanoic acids. Reference compounds were further characterized according to Fransson *et al.*[35] Overnight amidation at ambient temperature followed by extraction and pre-crystallization in ice-cold n-hexane yielded L-stereoisomer **1** in 80% yield and D-stereoisomer **2** in 55% yield.

Radiochemistry

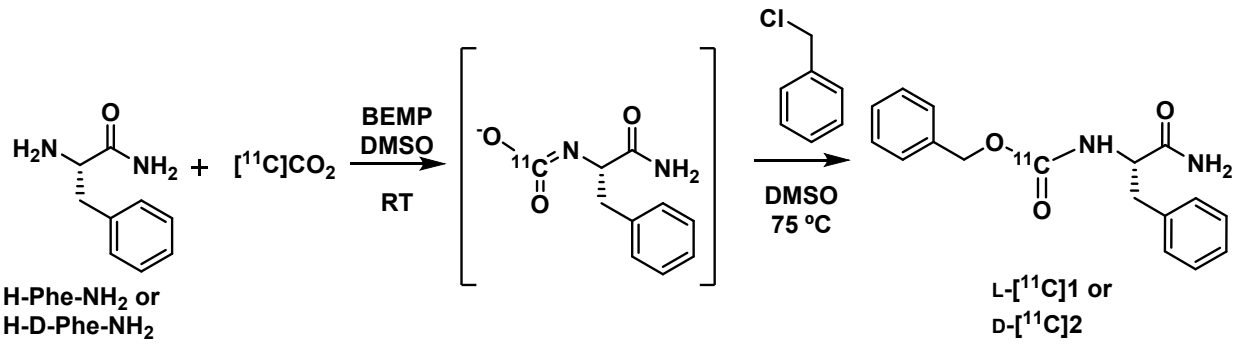

Scheme 1: Radiosynthesis of SP_{1-7} carbamate analogues [^{11}C]**1** and [^{11}C]**2**.

The general synthesis towards the SP_{1-7} carbamate analogues [^{11}C]**1** and [^{11}C]**2** is outlined in Scheme 1. The synthesis involved 2 steps: direct [^{11}C]CO_2 trapping at ambient temperature and ^{11}C-carboxybenzylation at elevated temperature. The preparation of SP_{1-7} carbamate analogue [^{11}C]**1**/[^{11}C]**2** was achieved without the isolation of the synthetic intermediate in a one-pot reaction to establish an efficient procedure for the desired product (Supporting Information; Table 1). In order to optimize this procedure, the following parameters have been thoroughly investigated: amount of reagents and solvent, reaction time and helium flow. These parameters were changed systematically one by one per experiment.

Trapping of cyclotron produced [^{11}C]CO_2 was >90%, when [^{11}C]CO_2 was bubbled thought the precursor solution in dry DMSO with the aid of 3.5 - 5.0 eq of 2-*tert*-butylimino-2-diethylamino-1,3-dimethylperhydro-1,3,2-diazaphosphorine (BEMP), which served as trapping reagent and a catalyst for the carboxylation reaction. The ^{11}C-carboxybenzylation to the desired product was achieved in high radiochemical yield (>85%; Supporting Information, Table 1), determined by analytical HPLC, using 4 - 5 eq of benzyl chloride, dissolved in DMSO, at 75 °C under helium stirring (10 mL·min^{-1}). Excellent conversion rates were attained for both reaction times of 5 and

10 min, whereas time of 5 min was selected to decrease the total synthesis time. The volume of DMSO was increased to 300 µL for a smoother automation of the synthesis procedure. Importantly, *N*-benzylation or other significant side products were not observed during the ^{11}C-carboxybenzylation reaction (Supporting Information; Figure 1).

The next step, purification of the PET-tracer was achieved using a reverse-phase C18 semi-preparative HPLC (Supporting Information; Figure 2 and 3). Subsequent reformulation towards an injectable solution provided [^{11}C]**1** (5.1 ± 2.2 GBq) in a radiochemical purity of >99% and A_M of 93.2 ± 46.9 GBq·µmol^{-1} in 23 - 29 min with an overall RCY of 27.9 ± 10.9% (corrected for decay; n=10) formulated in an *i.v.* injectable solution containing 10% EtOH in saline, ready for *in vivo* experiments.

In the same manner, we performed the reaction with H-D-Phe-NH_2 as precursor. As expected, the D-isomer displayed the same properties and the radiosynthesis of [^{11}C]**2** provided an isolated non-corrected yield of 3.9 ± 1.9 GBq (n=5) in a radiochemical purity of >99% and A_M of 69.4 ± 11.4 GBq·µmol^{-1} (n=4) in 26 - 29 min (n=5) with an overall RCY of 25.5 ± 9.7% (corrected for decay; n=5) formulated in an *i.v.* injectable solution (10% EtOH in saline).

Ex Vivo Biodistribution

In order to assess the brain and spinal cord penetration potential of [^{11}C]**1** an *ex vivo* biodistribution study was performed. Healthy male Wistar rats were injected with [^{11}C]**1** (25.8 ± 7.6 MBq; 0.74 ± 0.21 nmol; n=16) and were analyzed for biodistribution at 5, 15, 30 and 60 min post injection (*p.i.*) (Figure 2). [^{11}C]**1** was cleared via kidneys and liver, and showed moderate

uptake in well-perfused organs, like lungs and heart. Highest uptake was observed after 5 min in the brain regions (large brain, cerebellum, brain stem) and spinal cord, showing rapid penetration and BBB crossing of the SP_{1-7} peptidomimetic. At later time points we observed a better retention of the [^{11}C]**1** tracer in the spinal cord compared to the brain and the perfused organs.

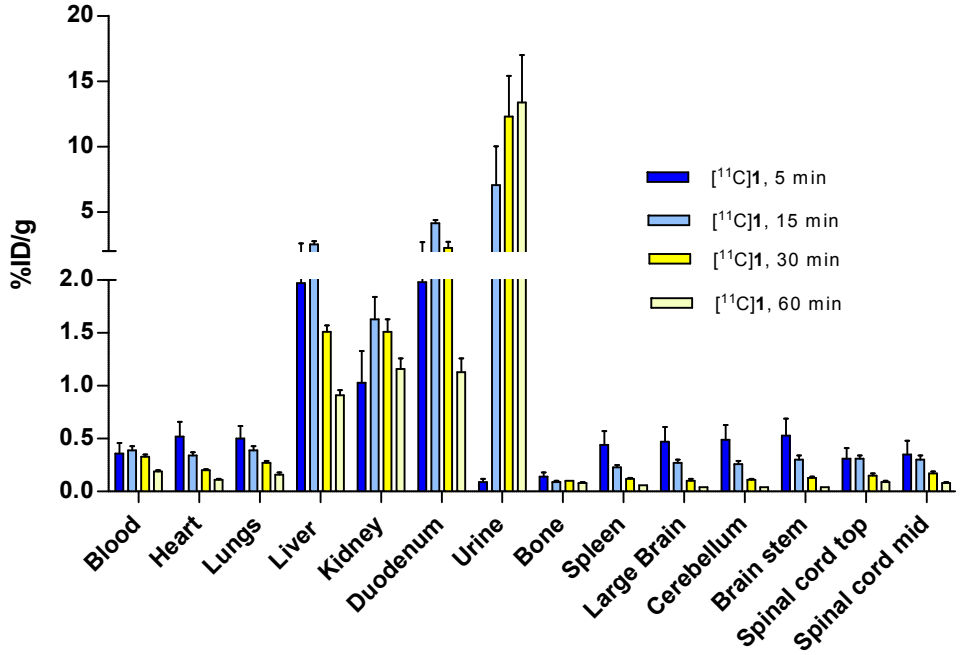

Figure 2: Biodistribution of [^{11}C]**1** at 5, 15, 30 and 60 min post-injection (*p.i.*) in healthy male Wistar rats (n=4 per time point) following *i.v.* administration of 25.8 ± 7.6 MBq (0.74 ± 0.21 nmol; n=16) of [^{11}C]**1** via the tail vein under isoflurane anesthesia (2 - 2.5% in 1 L·min^{-1}). Values are expressed in %ID/g ± SEM.

From the data obtained, organ of interest-to-blood ratios were also calculated (Figure 3A). The brain-to-blood ratios was 1.24 - 1.39 and spinal cord-to-blood ratios was 0.82 - 0.88 for [^{11}C]**1**.

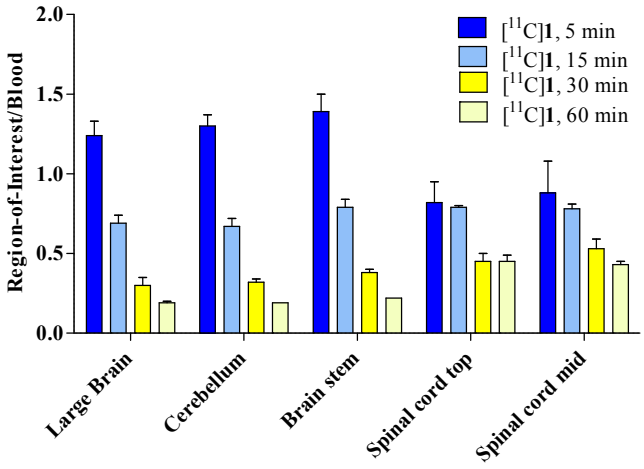

Figure 3: A: Organs-to-blood ratio of [^{11}C]**1** at 5, 15, 30 and 60 min (n=4 per time point).Columns show the region-of-interest to blood ratio ± SEM.

Metabolite Analysis (L-[^{11}C]1)

In vivo stability of [^{11}C]**1** was determined by metabolite analysis in healthy male Wistar rats (n=4 per time point). Rats were injected *i.v.* with the radiotracer [^{11}C]**1 (**27.3 ± 7.3 MBq; 0.50 ± 0.22 nmol; n=12) and sacrificed at 5, 15 and 45 min *p.i.* followed by blood sample collection and brain dissection. Analysis of the plasma revealed mediocre stability of the tracer with 52, 15 and 11% of intact tracer after 5, 15 and 45 min, respectively, suggesting extensive metabolic degradation (Table 1). HPLC analysis of the plasma showed the presence of one major metabolites of [^{11}C]**1** after 45 min. This major metabolite had a retention time of 12.7 min and constituted more than 67% of the non-polar metabolites (Figure 4). Radioactivity recovery of the blood samples was 99.1 ± 0.3, 70.0 ± 2.2 and 65.5 ± 3.7% at 5, 15 and 45 min, respectively. The Sep-Pak cartridge stickiness at later time points was inevitable, despite additional employment of MeOH.

In brain supernatant, the percentage of intact tracer in the non-polar fraction was >99.9% at 5 min and 97% after 15 or 45 min (Figure 4D). Radioactivity extraction of the brain supernatant samples was 77.1 ± 5.2, 71.5 ± 15.7 and 63.0 ± 5.9 % at 5, 15 and 45 min, respectively. These data confirms rapid penetration and stability of the [^{11}C]**1** tracer in brain.

Table 1: Metabolite analysis of [^{11}C]**1** in plasma, brain and spinal cord supernatant.

	Plasma			**Brain**			**Spinal Cord**
	5 min [%; SD]	**15 min [%; SD]**	**45 min [%; SD]**	**5 min [%; SD]**	**15 min [%; SD]**	**45 min [%; SD]**	**15 min [%]**
Intact tracer	52.3 ± 11.3	15.2 ± 7.9	10.9 ± 3.0	>99.9	97.3 ± 0.6	96.7 ± 4.5	97.6
Non-polar metabolite 1	7.8 ± 5.4	7.9 ± 2.4	7.7 ± 2.9	/	0.9 ± 0.6	1.6 ± 3.2	/
Non-polar metabolite 2	/	/	1.1 ± 1.1	/	/	/	/
Non-polar metabolite 3	34.3 ± 5.0	40.8 ± 4.4	40.0 ± 1.7	/	1.8 ± 0.2	1.6 ± 3.2	2.4
Polar metabolites	5.2 ± 1.1	6.1 ± 0.4	5.7 ± 0.3	/	/	/	/

Additionally, *in vivo* stability of [^{11}C]**1** in spinal cord was preliminary assessed by metabolite analysis in healthy male Wistar rats (n=4 per time point). Rats were injected *i.v.* with the radiotracer [^{11}C]**1** (32.8 ± 8.6 MBq; 0.63 ± 0.17 nmol; n=4) and sacrificed at 15 min *p.i.* followed by spinal cord dissection. Unfortunately, the percentage of the intact tracer in the spinal cord supernatant was possible to be assessed only for one rat (Supporting information), where results

indicate that [^{11}C]**1** is stable in spinal cord after 15 min, with a trace unidentified metabolite 2 (Supporting Information; Figure 4).

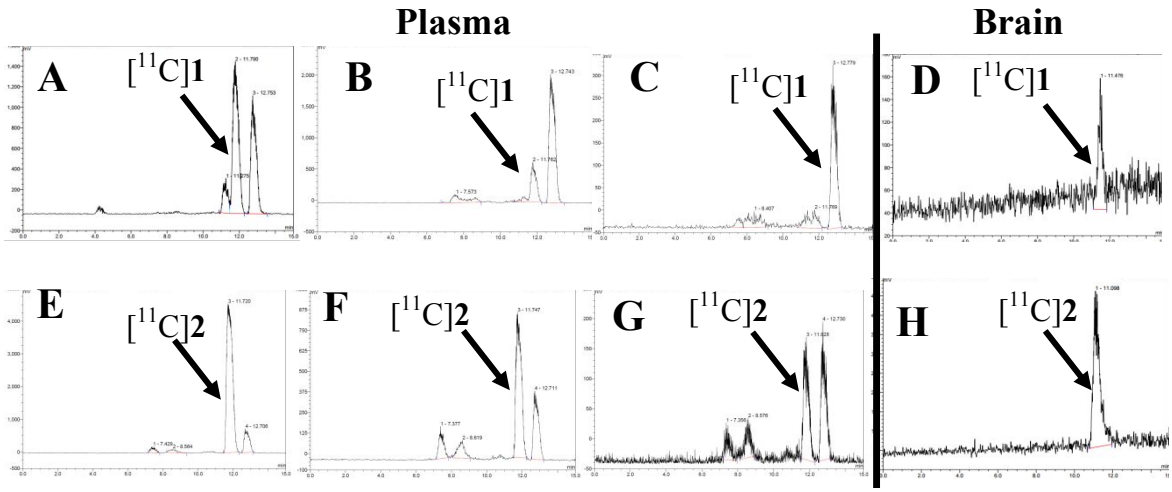

Figure 4: Metabolites radiochromatograms of the plasma non-polar fraction after: **A**: 5 min, **B**: 15 min and **C**: 45 min after L-[^{11}C]**1** injection; **E**: 5 min, **F**: 15 min and **G**: 45 min after D-[^{11}C]**2** injection. Intact L-[^{11}C]**1** and D-[^{11}C]**2** have a retention time of 11.7 min. Radiochromatograms of the total fraction of brain supernatant after 5 min showing presence of intact tracer: **D**: L-[^{11}C]**1** (R_t of 11.5 min); **H**: D-[^{11}C]**2** (R_t of 11.1 min). HPLC data has been corrected for decay.

Metabolite Analysis (D-[^{11}C]2)

In order to improve the bioavailability of the tracer we investigated the effect of substitution of L-phenylalanine to D-configuration. We synthesized the D-variant [^{11}C]**2** and examined the *in vivo* stability by metabolite analysis in healthy male Wistar rats (n=3 per time point). The rodents were injected *i.v.* with [^{11}C]**2** tracer (32.4 ± 3.4 MBq; 1.80 ± 0.19 nmol; n=9) and rats were sacrificed at 5, 15 and 45 min *p.i.* followed by blood collection and brain dissection. Plasma analysis revealed improved stability of the tracer with 80, 49 and 37% of intact tracer after 5, 15 and 45 min, respectively (Table 3). Radioactivity recovery of the blood samples was 95 - 99% at all time points.

HPLC analysis of non-polar fraction revealed three unidentified metabolites (Figure 4E-G, and Table 3).

Table 2: Metabolite analysis of D-isomer [^{11}C]**2** in plasma and brain supernatant.

	Plasma			Brain		
	5 min [%; SD]	**15 min [%; SD]**	**45 min [%; SD]**	**5 min [%; SD]**	**15 min [%; SD]**	**45 min [%; SD]**
Intact tracer	79.6 ± 2.3	49.2 ± 2.0	36.6 ± 1.7	96.4 ± 6.3	96.4 ± 5.2	>99.9
Non-polar metabolite 1	2.6 ± 0.2	9.8 ± 0.8	10.5 ± 4.8	3.6 ± 6.3	3.6 ± 5.2	/
Non-polar metabolite 2	1.8 ± 0.6	9.5 ± 1.3	7.2 ± 3.0	/	/	/
Non-polar metabolite 3	11.3 ± 1.1	20.9 ± 1.5	33.6 ± 0.2	/	/	/
Polar metabolites	3.5 ± 0.5	5.6 ± 0.9	7.3 ± 2.0	/	/	/

In brain supernatant, the percentage of intact D-[^{11}C]**2** tracer in the non-polar fraction was >96% after 5, 15 and 45 min (Figure 4B, H). Radioactivity extraction of the brain supernatant samples was 58.8 ± 13.7, 55.1 ± 22.0 and 63 ± 13.3% at 5, 15 and 45 min, respectively.

LC-MS/MS Method

A product ion scan was performed for **1** to determine high intensity mass fragments in a multiple reaction monitoring (MRM) method by LC-MS/MS experiments. The transition of 299.1 *m/z* to 255.1 was chosen where the fragments corresponded to the intact parent ion and a loss of carboxylic fragment, and the transition of 315.1 *m/z* to 271.1 was chosen where the fragments

corresponded to the hydroxylated parent ion and a loss of carboxylic fragment. Non-polar plasma fractions, after 5 and 15 min *p.i*, were analyzed demonstrating a trace amount of **2** (Supporting Information, Figure 5; blue trace) and two mass peaks of 315.1 (Supporting Information, Figure 5; red trace) corresponding to the hydroxylated parent ion.

Additionally, the transition of 475.1 *m/z* to 299.1 was chosen to detect the glucoronated parent ion and the intact parent ion. Rat was pretreated with cold non-radiolabeled **1,** injected 5 min before PET scan as a blocker, where non-polar plasma sample indeed confirmed the glucorinated metabolite after 60 min [^{11}C]**1** *p.i.* (Supporting Information, Figure 5, green trace). Furthermore, using this transition the non-polar plasma samples from *in vivo* stability study of [^{11}C]**2** were re-analyzed, confirming the postulated metabolites (hydroxylation, oxidative deamination and subsequent glucoronidation) (Supporting Information; Scheme 2).

PET Imaging

Dynamic PET imaging was carried out in healthy rats with [^{11}C]**1** and [^{11}C]**2** tracers (Figure 5). The time-activity-curves (TACs) of the PET imaging showing SUVs over time are presented in Figure 6. Under baseline condition [^{11}C]**1** scan revealed good uptake in the brain, reaching a maximum of 1.5 ± 0.05 SUV (n=4) at 3 min *p.i*., followed by a rapid clearance within 60 min. [^{11}C]**1** showed consistent uptake in the brain with no variation between different rats (Figure 6A). In the spinal cord (Figure 6F) the maximum uptake was at 10 min *p.i* and reached 0.95 ± 0.03 SUV (n=4).

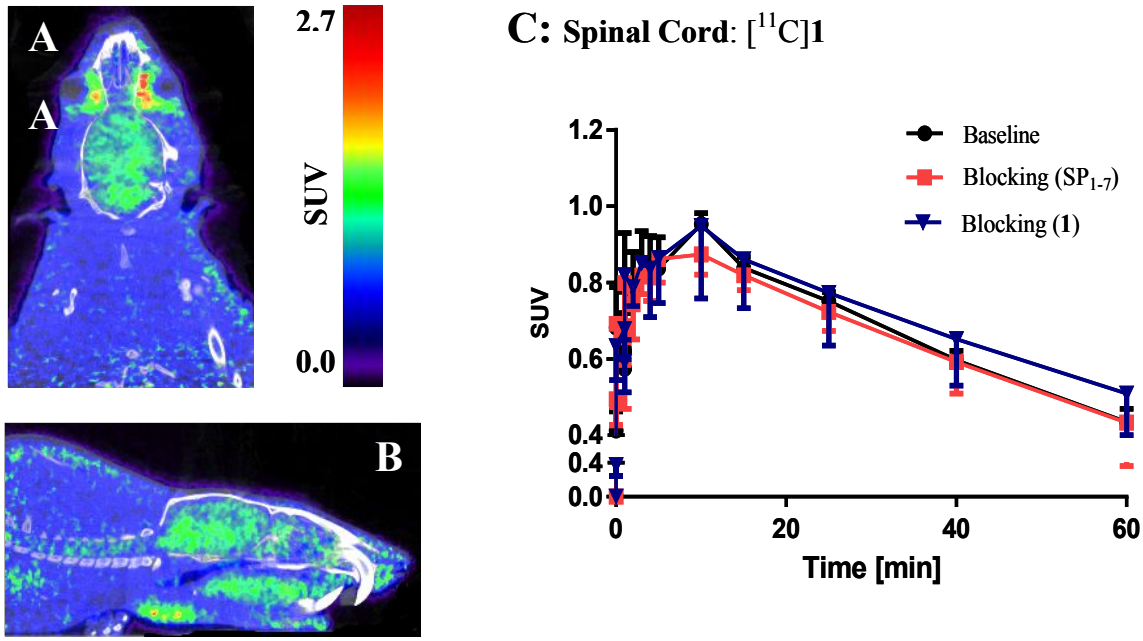

Figure 5: Static reconstruction of the PET-image scans in healthy male Wistar rat (Rat 2) with tracer [^{11}C]**1** (20 MBq *i.v.* injection via tail vein; 3% and 1 – 2.5% isoflurane in oxygen (1 L·min-1) for induction and maintenance). **A**: PET/CT between 0 - 60 min coronal image. **B**: PET/CT between 0 - 60 min sagittal image. **C**: Time-activity-curves (TACs) of [^{11}C]**1** expressed as SUV ± SD. TACs of non-blocking (black line) and blocking conditions (colored lines): natural SP_{1-7} administered 15 min before [^{11}C]**1** (red line; n=2) and compound **1** 20 min prior to tracer injection (blue line; n=2).

In order to verify the specific uptake in brain, blocking experiments were performed. Pretreatment with natural SP_{1-7} (15 min, *i.p.*, 185 nmol·kg^{-1}) or cold compound **1** (20 min prior to tracer injection, *i.v.*, 3 µmol·kg^{-1}) did not block brain uptake. Although, when **1** was injected 3 min prior to tracer injection (*i.v.*, 3 µmol·kg^{-1}), we noticed an increase in the SUV up to 2.0 at 3 min.

Despite our efforts to block brain uptake [^{11}C]**1**, pretreatment did not measurably decrease radiotracer uptake resulting in similar uptake pattern for all scans (Figure 6B and E).

In the spinal cord pretreatment with the natural SP_{1-7} showed moderate blocking (0.95 SUV baseline condition vs 0.87 SUV block) (Figure 5C, black vs. red line). However, self-blocking with **1** at 3 or 20 min prior tracer injection did not show any blocking (Figure 5C, blue line).

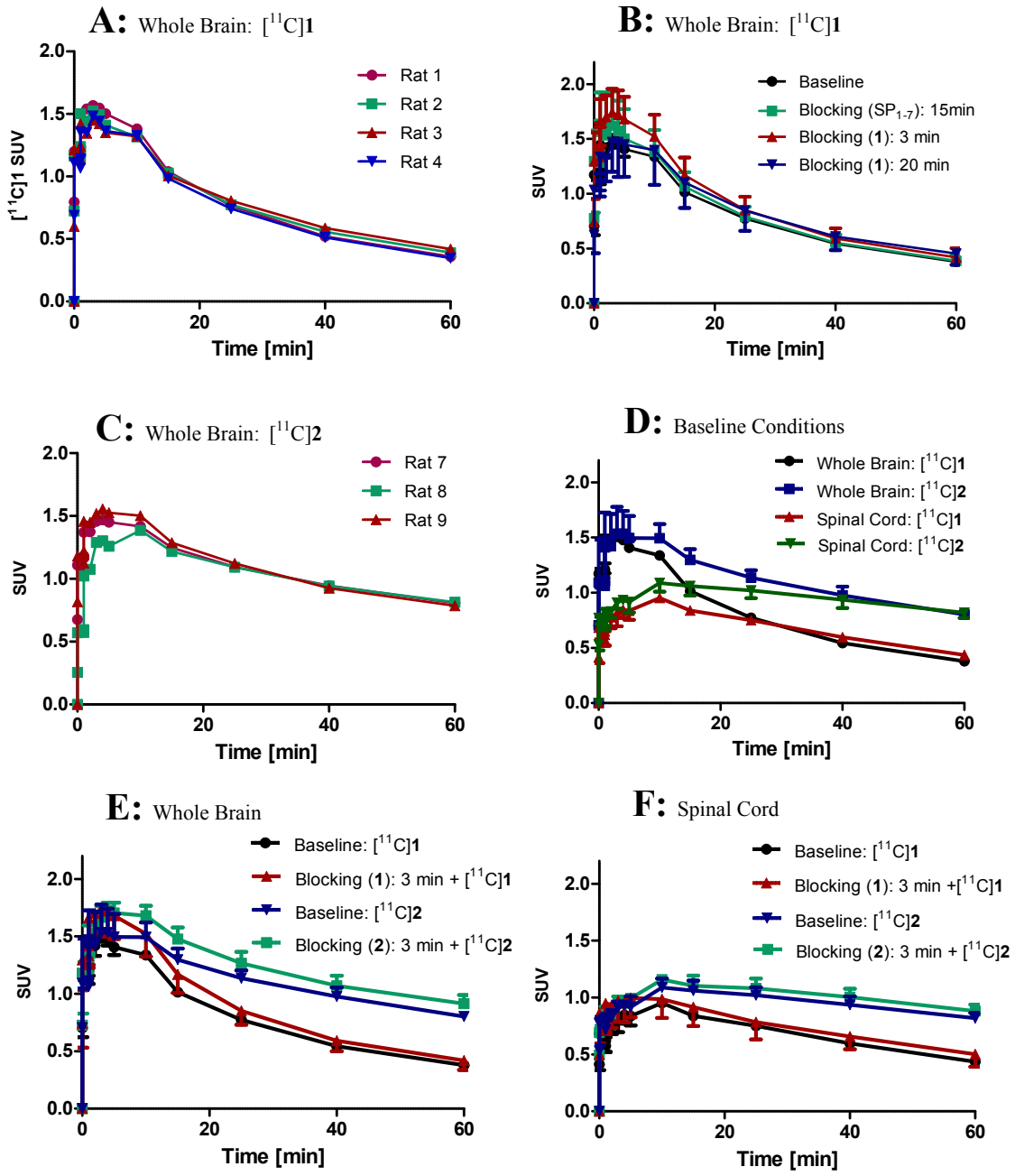

Figure 6: Time-activity-curves (TACs) of [^{11}C]**1** and [^{11}C]**2** in healthy male Wistar rats expressed in SUV ± SD (region of interest around the brain and spinal cord were drawn manually). **A**: TACs of whole brain with tracer [^{11}C]**1**. **B**: TACs of non-blocking and blocking conditions with tracer [^{11}C]**1**. **C**: TACs of whole brain with tracer [^{11}C]**2**. **D**: TACs of whole brain regions and spinal

cord (top part) of [^{11}C]**1** or [^{11}C]**2**. **E**: TACs under a baseline and self-blocking conditions for [^{11}C]**1** and [^{11}C]**2** in whole brain. **F**: TACs under a baseline and self-blocking conditions for [^{11}C]**1** and [^{11}C]**2** in spinal cord (top part).

The uptake pattern of D-[^{11}C]**2** in brain and spinal cord was different compared to L-[^{11}C]**1**. At early time points (before 5 min) the level of uptake was comparable between the two tracer, but at later time points D-[^{11}C]**2** displayed slower clearance (SUV difference of app. 0.4 at 60 min; Figure 6D - blue and green line) and higher retention in brain and spinal cord. Self-blocking with compound **2** (3 min prior TOI, *i.v.*, 3 μmol·kg^{-1}) did not show any blocking effect in brain and spinal cord (brain - peak uptake at 3 min: SUV baseline 1.5 vs block 1.7; spinal cord - peak uptake at 10 min: SUV baseline 0.95 vs block 1.0) (Figure 6E and F).

Discussion

The dipeptide H-Phe-Phe-NH_2 has been previously recognized as a small molecule ligand for the $SP_{1\text{-}7}$ binding site with intriguing effect on neuropathic pain after central administration in rats. Herein, we introduce two $SP_{1\text{-}7}$ carbon-11 labeled benzylacarbamate peptidomimetics, L-[^{11}C]**1** and its D-analogue [^{11}C]**2**, derived from the lead dipeptide, and their preliminary *in vivo* and *ex vivo* evaluation. In particular, we exploited two carbon-11 labeled $SP_{1\text{-}7}$ ligands as radiotracers for a new target for PET imaging.

To facilitate the discovery of novel CNS PET ligands and to confirm the rationale for the PET ligand discovery process we employed a novel tool CNS PET MPO and commercial *in silico*

prediction platform. Both models supported the brain penetration and consequently, the carbon-11 labeled SP_{1-7} peptidomimetics L-[^{11}C]**1** and D-[^{11}C]**2** were successfully accomplished in an automated radiosynthesis with excellent yields, purities and molar activities.

Even though the *in vitro* plasma stability and permeability assay of L-**1** have been reported, *in vivo* evaluation is eagerly awaited. Initial *in vivo* biodistribution study of [^{11}C]**1** in healthy rats displayed desired uptake in large brain, cerebellum and brain stem, as well as in spinal cord.

The metabolic stability of the [^{11}C]**1** was less optimal with fast degradation in the plasma, generally known for peptides. However, in the brain and spinal cord [^{11}C]**1** showed high stability with more than 95% of intact tracer, suggesting that the degradation of [^{11}C]**1** is mainly due to the peptidase and proteases present in the blood. This claim is further supported by the significant increase of plasma stability when the L-Phe for its D-isomer ([^{11}C]**2**). On a positive note the [^{11}C]**1** metabolites did not cross the BBB or the BSCB, which support the potential of the molecule as a PET tracer. The metabolite data for for L- and D-carbamate tracers ([^{11}C]**1** and [^{11}C]**2**) showed similar HPLC chromatogram pattern, suggesting identical metabolic pathway towards several unknown non-polar metabolites. These results are in line with the data reported by Fransson *et al.* in 2014[35].

To further evaluate the stability of the two tracers, xenobiotic metabolism (phase I) was anticipated using freely available MetaPrint 2D tool, which predicts metabolism through data-mining and statistical analysis of known metabolic transformations reposted in the literature (Supporting Information; Scheme 2). Based on this prediction, we postulated that the observed

metabolites with shorter retention times on chromatograms Figure 3 might be the hydroxylated [^{11}C]**1**/[^{11}C]**2** on one of the aromatic rings. In order to test the hypothesis, additional LC-MS/MS experiments were performed as the methodology allows detection of the carrier amounts of ions involved in high molar activity PET-tracers. A product ion scan analysis of non-polar plasma fractions demonstrated a trace amount of **1** (Supporting Information; Figure 5; blue) and two mass peaks of the hydroxylated parent ion (Supporting Information; Figure 5; red), but unfortunately, it was not possible to identify is it was the phenylalanine or the carboxybenzyl hydroxylates. For the most abundant metabolite that increased rapidly overtime (Figure 3), we hypothesized that is a glucuronidation of the compound.

Glucuronidation is known as the most important phase II metabolic pathway responsible for the clearance of many endogenous and exogenous compounds.[37] Qualitative assessment using this MS/MS transition method of predicted metabolites with non-polar plasma sample confirmed the glucorinated metabolite of [^{11}C]**1** (Supporting Information; Figure 5, green). In addition, the non-polar plasma samples from *in vivo* stability study of [^{11}C]**2** were re-analyzed (Supporting Information; Figure 5), all confirming postulated metabolites - a hydroxylation, oxidative deamination or/and glucoronidation reaction. To clarify the position of the peaks, the glucoronated metabolite this time showed less retention on Kinetex Biphenyl column compared to the parent ion, due to glucuronide moiety possessing less pi-electrons. These results suggest that glucuronic acid is transferred to another nucleophilic atom in acceptor parent molecule, where most likely *O*-linked moiety (e.g. activation of the carboxylic group in phase I) would be the most preferred functional group for the reaction.

PET imaging with both compounds revealed rapid and homogenous uptake throughout the brain and in the spinal cord followed by fast clearance (Figure 6A and 6D). Maximum accumulation of [^{11}C]**1** in brain was detected 3 min *p.i.* and after 10 min in spinal cord. Relatively fast clearance and liver and kidney uptake could be also attributed to [^{11}C]**1** potentially being bound to plasma proteins.[11] Superior plasma stability of D-analogue [^{11}C]**2** was reflected in PET imaging by higher accumulation and slower clearance pattern from the brain and spinal cord which suggests that [^{11}C]**2** is a better imaging PET tracer than [^{11}C]**1.**

Blocking experiments with natural heptapeptide SP_{1-7}, injected *i.p.* 15 min prior to tracer [^{11}C]**1** administration, did not show difference in brain between baseline and blocking scan (Figure 6B). The poor BBB permeability, stability of peptides *in vivo*, difference between the binding in brain and spinal cord[12,13] (SP_{1-7}: rat spinal cord membrane: 1.6 nM, vs. rat ventral tegmental area: 3.9 nM) are a possible reason. Furthermore, a publication by Skogh *et al.*[7] published very shortly after we conducted PET scans, revealed the SP_{1-7} *in vitro* half-life in mouse plasma of 4.4 min, which further explain the lack of blocking in brain. Intriguing, a minor blocking was observed in the spinal cord with decreased SUV values (from 0.95 to 0.87, Figure 5C - black vs. red line. This observation can be supported by the Skogh's publication[7] where they confirmed anti-allodynic effect of SP_{1-7} observed after *i.p.* administration. It should be mentioned that we have used the same dose and way of administration for our blocking studies as Skogh. Surprisingly, this centrally located target was confirmed by the fact that homogenate of spinal cord was used for their *in vitro* binding studies, but SP_{1-7} failed to display any measurable permeability in the Caco-2 cell monolayer.[7] Pretreatment with non-radioactive **1,** injected *i.v.* in the tail vein 20 min prior to [^{11}C]**1**, affected no measurable change in whole brain radioactivity uptake. Considering low metabolic

stability unveiled during this investigation, non-radioactive **1** was also injected only 3 min prior to tracer [^{11}C]**1**, where we observed in brain an increase of the SUV values up to 2.0. This might be explained by the fact that the pretreatment with non-labeled compound, also subjected to rapid xenobiotic metabolism, preserves more of the intact [^{11}C]**1** in the blood for BBB and BSCB penetration. Further, self-blocking by pretreatment of **1** resulted in unaltered SUV values at 10 min, while SUV values for injection 3 min prior TOI were slightly increased at 3 min, compared to baseline SUV values (Figure 5C; blue line).

In summary, self-blocking studies showed no specific binding in whole brain and spinal cord of [^{11}C]**1** over the duration of the scan (Figure 6E and 6F). In comparison, self-blocking with non-radioactive **2** prior injection of [^{11}C]**2** resulted in increased SUV values for brain regions and almost unaffected SUV values for spinal cord (top part; Figure 6E and 6F). It can be concluded that peptides, in particular $SP_{1\text{-}7}$, show significant sensitivity to peptidases degradation. Further, increased permeability of the BSCB compared to BBB[38] might explain our blocking only in the spinal cord with $SP_{1\text{-}7}$. Worth mentioning in this context is also that BBB and BSCB passage can be affected by the disease model, e.g. peripheral nerve injury, used for studying neuropathic pain[39], compared to the healthy animal rats.

Taken together, rapid brain and spinal cord uptake of [^{11}C]**1** and [^{11}C]**2** not only confirms sufficient BBB and BSCB exposure, but also indicates that both L- and D-tracers are not likely to be a substrates for efflux transporters, as it has been indicated for other H‑Phe-Phe-NH_2 analogues by Fransson[16]. These initial studies showed that both candidates have good tracer properties, such as excellent metabolic stability in the brain and spinal cord and favorable pharmacokinetics with

a maximum brain and spinal cord concentration app. 3 min and 10 min, respectively, after bolus injection in rats, all important considerations for imaging of CNS. Further validation of the tracer candidates in the disease model is necessary to overcome the poor understanding of SP_{1-7} binding site on molecular level, which hampers employment of appropriate blocking compounds.

Conclusion

In summary, an efficient and high yielding radiochemistry was exploited to develop two SP_{1-7} ^{11}C-benzylacarbamates **1** and **2**. *In silico* commercial model and CNS PET MPO algorithm were able to predict the brain- and spinal cord-permeable radiotracer(s). Preclinical evaluation characterizing the metabolic stability, biodistribution and *in vivo* PET imaging profile, confirmed that peptidomimetics **1** and **2** enter the rodent brain and spinal cord. Altogether, these encouraging data suggest a promising starting point for further tracer validation.

Supporting Information

List of abbreviations; Prediction model results; Chemical synthesis – control reaction, Radiochemistry - optimization, HPLC chromatograms; Metabolite analysis – spinal cord, LC-MS/MS spectra; Metabolism prediction; Program for automated synthesis; Mass calibration curve data.

Author Information

Corresponding Author

* Prof.dr. Albert D. Windhorst, Radionuclide Center, Department of Radiology and Nuclear Medicine, VU University Medical Center, De Boelelaan 1085c, 1081 HV Amsterdam, the Netherlands. E-mail: ad.windhorst@vumc.nl

Author Contributions

The manuscript was written through contributions of all authors. All authors have given approval to the final version of the manuscript. §: These authors contributed equally to this work.

Acknowledgements

The research leading to these results has been financially supported by the European Marie Curie Actions RADIOMI Initial Training Network (FP7-PEOPLE-2012-ITN) under project reference no. 316882. BV Cyclotron VU (Amsterdam) is acknowledged for providing [11C]CO2.

Conflict of interest

The authors report no conflict of interest.

References

(1) Jonsson, A.; Fransson, R.; Haramaki, Y.; Skogh, A.; Brolin, E.; Watanabe, H.; Nordvall, G.; Hallberg, M.; Sandström, A.; Nyberg, F. Small Constrained SP1-7 Analogs Bind to a Unique Site and Promote Anti-Allodynic Effects Following Systemic Injection in Mice. *Neuroscience* **2015**, *298*, 112–119.

(2) Franzen, H. M.; Ragnarsson, U. Preperation and 11C-Labelling of a Substance P Analogue

Containing D-Tryptophan in Positions 7 and 9. *J. Chem. Soc.* **1988**, *1*, 497–502.

(3) Wolfensberger, S. P. A.; van Berckel, B. N. M.; Airaksinen, A. J.; Maruyama, K.; Lubberink, M.; Boellaard, R.; Carey, W. D. H.; Reddingius, W.; Veltman, D. J.; Windhorst, A. D.; et al. First Evaluation of [11C]R116301 as an in Vivo Tracer of NK1 Receptors in Man. *Mol. Imaging Biol.* **2009**, *11* (4), 241–245.

(4) Hargreaves, R.; Ph, D. Imaging Substance P Receptors (NK1) in the Living Human Brain Using Positron Emission Tomography. *Psychiatry Interpers. Biol. Process.* **2002**, *63*, 18–24.

(5) Fransson, R.; Botros, M.; Sköld, C.; Nyberg, F.; Lindeberg, G.; Hallberg, M.; Sandström, A. Discovery of Dipeptides with High Affinity to the Specific Binding Site for Substance P1-7. *J. Med. Chem.* **2010**, *53* (6), 2383–2389.

(6) Abba J. Kastin. *Handbook of Biologically Active Peptides*; 2013.

(7) Skogh, A.; Lesniak, A.; Gaugaz, F. Z.; Svensson, R.; Lindeberg, G.; Fransson, R.; Nyberg, F.; Hallberg, M.; Sandström, A. Importance of N- and C-Terminal Residues of Substance P 1-7 for Alleviating Allodynia in Mice after Peripheral Administration. *Eur. J. Pharm. Sci.* **2017**, *106*, 345–351.

(8) Zhou, Q.; Liu, Z.; Ray, A.; Huang, W.; Karlsson, K.; Nyberg, F. Alteration in the Brain Content of Substance P (1-7) during Withdrawal in Morphine-Dependent Rats. *Neuropharmacology* **1998**, *37* (12), 1545–1552.

(9) Botros, M.; Hallberg, M.; Johansson, T.; Zhou, Q.; Lindeberg, G.; Frändberg, P. A.; Tömböly, C.; Tóth, G.; Le Grevès, P.; Nyberg, F. Endomorphin-1 and Endomorphin-2

Differentially Interact with Specific Binding Sites for Substance P (SP) Aminoterminal SP1-7 in the Rat Spinal Cord. *Peptides* **2006**, *27* (4), 753–759.

(10) Botros, M.; Johansson, T.; Zhou, Q.; Lindeberg, G.; Tömböly, C.; Tóth, G.; Le Grevès, P.; Nyberg, F.; Hallberg, M. Endomorphins Interact with the Substance P (SP) Aminoterminal SP1-7binding in the Ventral Tegmental Area of the Rat Brain. *Peptides* **2008**, *29* (10), 1820–1824.

(11) Fransson, R.; Nordvall, G.; Bylund, J.; Carlsson-Jonsson, A.; Kratz, J. M.; Svensson, R.; Artursson, P.; Hallberg, M.; Sandstro, A. Exploration and Pharmacokinetic Profiling of Phenylalanine Based Carbamates as Novel Substance P1−7 Analogues. *ACS Med. Chem. Lett.* **2014**, *5* (1), 1272–1277.

(12) Fransson, R.; Botros, M.; Nyberg, F.; Lindeberg, G.; Sandström, A.; Hallberg, M. Small Peptides Mimicking Substance P (1-7) and Encompassing a C-Terminal Amide Functionality. *Neuropeptides* **2008**, *42* (1), 31–37.

(13) Zhou, Q.; Carlsson, A.; Botros, M.; Fransson, R.; Sandstr??m, A.; Gordh, T.; Hallberg, M.; Nyberg, F. The C-Terminal Amidated Analogue of the Substance P (SP) Fragment SP1-7 Attenuates the Expression of Naloxone-Precipitated Withdrawal in Morphine Dependent Rats. *Peptides* **2009**, *30* (12), 2418–2422.

(14) Botros, M.; Hallberg, M.; Johansson, T.; Zhou, Q.; Lindeberg, G.; Fra, P. Endomorphin-1 and Endomorphin-2 Differentially Interact with Specific Binding Sites for Substance P (SP) Aminoterminal SP 1–7 in the Rat Spinal Cord. *Peptides* **2006**, *27*, 753–759.

(15) Igwe, O. J.; Kim, D. C.; Seybold, V. S.; Larson, a a. Specific Binding of Substance P

Aminoterminal Heptapeptide [SP(1-7)] to Mouse Brain and Spinal Cord Membranes. *J. Neurosci.* **1990**, *10* (11), 3653–3663.

(16) Fransson, R.; Sköld, C.; Kratz, J. M.; Svensson, R.; Artursson, P.; Nyberg, F.; Hallberg, M.; Sandström, A. Constrained H-Phe-Phe-NH2 Analogues with High Affinity to the Substance P 1-7 Binding Site and with Improved Metabolic Stability and Cell Permeability. *J. Med. Chem.* **2013**, *56* (12), 4953–4965.

(17) R., B.; Baron, R. Mechanisms of Disease: Neuropathic Pain - A Clinical Perspective. *Nat. Clin. Pract. Neurol.* **2006**, *2* (2), 95–106.

(18) Colloca, L.; Ludman, T.; Bouhassira, D.; Baron, R.; Dickenson, A. H.; Yarnitsky, D.; Freeman, R.; Truini, A.; Attal, N.; Finnerup, N. B.; et al. Neuropathic Pain. *Nat. Rev. Dis. Prim.* **2017**, *3*, 17002.

(19) Gunn, R. N.; Rabiner, E. A. Imaging in Central Nervous System Drug Discovery. *Semin. Nucl. Med.* **2017**, *47* (1), 89–98.

(20) Lever, S. Z.; Fan, K. H.; Lever, J. R. Tactics for Preclinical Validation of Receptor-Binding Radiotracers. *Nucl. Med. Biol.* **2017**, *44*, 4–30.

(21) Miller, P. W.; Long, N. J.; Vilar, R.; Gee, A. D. Synthesis of 11 C, 18 F, 15 O, and 13 N Radiolabels for Positron Emission Tomography. *Angew. Chemie Int. Ed.* **2008**, *47* (47), 8998–9033.

(22) Dahl, K.; Halldin, C.; Schou, M. New Methodologies for the Preparation of Carbon-11 Labeled Radiopharmaceuticals. *Clin. Transl. Imaging* **2017**, *5* (3), 275–289.

(23) Antoni, G. Development of Carbon-11 Labelled PET Tracers-Radiochemical and Technological Challenges in a Historic Perspective. *J. Label. Compd. Radiopharm.* **2015**, *45*, 65–72.

(24) Wadsak, W.; Mitterhauser, M. Basics and Principles of Radiopharmaceuticals for PET/CT. *Eur. J. Radiol.* **2010**, *73* (3), 461–469.

(25) Vallabhajosula, S.; Solnes, L.; Vallabhajosula, B. A Broad Overview of Positron Emission Tomography Radiopharmaceuticals and Clinical Applications: What Is New? *Semin. Nucl. Med.* **2011**, *41* (4), 246–264.

(26) Rotstein, B. H.; Liang, S. H.; Placzek, M. S.; Hooker, J. M.; Wilson, A. A.; Vasdev, N. 11C=O Bonds Made Easily for Positron Emission Tomography Radiopharmaceuticals. *Chem. Soc. Rev.* **2016**, *45* (17), 4708–4726.

(27) Pekošak, A.; Rotstein, B. H.; Collier, T. L.; Windhorst, A. D.; Vasdev, N.; Poot, A. J. Stereoselective ^{11}C-Labeling of a "Native" Tetrapeptide Using Asymmetric Phase-Transfer Catalyzed Alkylation Reactions. *European J. Org. Chem.* **2017**, *2017* (5), 1019–1024.

(28) Miller, P. W.; Long, N. J.; Vilar, R.; Gee, A. D. Synthesis of 11C, 18F, 15O, and 13N Radiolabels for Positron Emission Tomography. *Angew. Chem. Int. Ed. Engl.* **2008**, *47* (47), 8998–9033.

(29) Hooker, J. M.; Reibel, A. T.; Hill, S. M.; Schueller, M. J.; Fowler, J. S. One-Pot, Direct Incorporation of [11C]CO2 into Carbamates. *Angew. Chemie - Int. Ed.* **2009**, *48* (19), 3482–3485.

(30) Wilson, A. a; Garcia, A.; Houle, S.; Vasdev, N. Direct Fixation of [(11)C]-CO(2) by

Amines: Formation of [(11)C-Carbonyl]-Methylcarbamates. *Org. Biomol. Chem.* **2010**, *8* (2), 428–432.

(31) Zhang, L.; Villalobos, A.; Beck, E. M.; Bocan, T.; Chappie, T. A.; Chen, L.; Grimwood, S.; Heck, S. D.; Helal, C. J.; Hou, X.; et al. Design and Selection Parameters to Accelerate the Discovery of Novel Central Nervous System Positron Emission Tomography (PET) Ligands and Their Application in the Development of a Novel Phosphodiesterase 2A PET Ligand. *J. Med. Chem.* **2013**, *56*, 4568–4579.

(32) Zhang, L.; Villalobos, A. Strategies to Facilitate the Discovery of Novel CNS PET Ligands. *EJNMMI Radiopharm. Chem.* **2016**, *1*, 1–12.

(33) Wager, T. T.; Hou, X.; Verhoest, P. R.; Villalobos, A. Moving beyond Rules: The Development of a Central Nervous System Multiparameter Optimization (CNS MPO) Approach To Enable Alignment of Druglike Properties. **2010**, 435–449.

(34) Windhorst, A. D.; ter Linden, T.; de Nooij, A.; Keus, J. F.; Buijs, F. L.; Schollema, P. E.; van Rooij, L. F.; Herscheid, J. D. M. A Complete, Multipurpose, Low Cost, Fully Automated and GMP Compliant Radiosynthesis System. *J Label Compd Radiopharm* **2001**, *44* (S1), S1052--S1054.

(35) Fransson, R.; Nordvall, G.; Bylund, J.; Carlsson-Jonsson, A.; Kratz, J. M.; Svensson, R.; Artursson, P.; Hallberg, M.; Sandstro, A. Exploration and Pharmacokinetic Pro Fi Ling of Phenylalanine Based Carbamates as Novel Substance P 1 − 7 Analogues. *ACS Med. Chem. Lett.* **2014**, *5*, 1272–1277.

(36) Murata, T.; Umeda, M.; Yoshikawa, S.; Urbahns, K.; Gupta, J.; Osamu, S. WO2004043926

(A1) - PHENYL OR HETEROARYL AMINO ALKANE DERIVATIVES AS IP RECEPTOR ANTAGONIST, 2004.

(37) Ge, S.; Tu, Y.; Hu, M. Challenges and Opportunities with Predicting In Vivo Phase II Metabolism via Glucuronidation From In Vitro Data. *Curr. Pharmacol. Reports* **2016**, *2* (6), 326–338.

(38) Bartanusz, V.; Jezova, D.; Alajajian, B.; Digicaylioglu, M. The Blood-Spinal Cord Barrier: Morphology and Clinical Implications. *Ann. Neurol.* **2011**, *70* (2), 194–206.

(39) Jaggi, A. S.; Jain, V.; Singh, N. Animal Models of Neuropathic Pain. *Fundam. Clin. Pharmacol.* **2011**, *25* (1), 1–28.

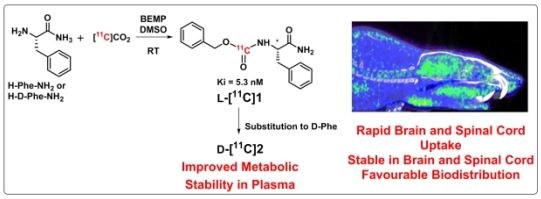

1034x383mm (96 x 96 DPI)